01 Jul 2003

One-Step Processing of Spinel Ferrites via the High-Energy Ball Milling of Binary Oxides

V. G. Harris

D. J. Fatemi

J. O. Cross

E. E. Carpenter

et. al. For a complete list of authors, see https://scholarsmine.mst.edu/chem_facwork/916

Recommended Citation

V. G. Harris et al., "One-Step Processing of Spinel Ferrites via the High-Energy Ball Milling of Binary Oxides," *Journal of Applied Physics*, vol. 94, no. 1, pp. 496-501, American Institute of Physics (AIP), Jul 2003.

The definitive version is available at https://doi.org/10.1063/1.1577225

One-step processing of spinel ferrites via the high-energy ball milling of binary oxides

V. G. Harris,[a] D. J. Fatemi, J. O. Cross, E. E. Carpenter, and V. M. Browning
U.S. Naval Research Laboratory, Washington, D.C. 20375

J. P. Kirkland
SFA, Inc., Landover, Maryland 20785

Amitabh Mohan and Gary J. Long
Department of Chemistry, University of Missouri-Rolla, Rolla, Missouri 65409-0010

(Received 3 February 2003; accepted 1 April 2003)

MnZn ferrites have been produced via the high-energy ball milling of binary oxide precursors. The milled ferrites have a nonequilibrium cation site distribution, with an unusually high population of Zn cations on the octahedral sites. The particle size distribution drops precipitously with milling time from 60 ± 1 to $\sim14\pm1$ nm at 10 h, but increases to 18.5 ± 1 nm after long durations (20–40 h) concurrent with the formation of nearly pure ferrite. A 1 h anneal at 673 K facilitates a redistribution of cations to their near equilibrium sites. This processing approach circumvents the need for deleterious high-temperature heat treatments that often lead to nonstoichiometries in the resulting ferrites. © *2003 American Institute of Physics.* [DOI: 10.1063/1.1577225]

INTRODUCTION

Traditional ferrite fabrication processes involve the repeated firing and grinding of binary oxide mixtures until a nearly pure spinel phase is formed.[1] In these processes, solid-state transformation occurs during the high temperature anneals, while grinding is employed to promote homogeneity. These approaches often suffer from nonstoichiometries that arise from the vaporization of constituents having low vapor pressures. As such, one goal of modern ferrite research and development has been to identify processing schemes that do not rely upon high temperature anneals for solid-state reactions.[2]

In this article, we report the single-step processing of MnZn ferrite via the high-energy ball milling (HEBM) of binary oxide precursors. This technique offers several advantages over traditional processing approaches, including low-temperature solid-state reactions, fewer processing steps, and a closed processing volume that minimizes exposure of toxic materials to the operator and eliminates any possibility of constituent loss to the environment.[3] Disadvantages of using this approach include the formation of ferrites having a non-equilibrium distribution of cations, a high density of defects, and contamination by the ball and cylinder materials. We have found that a low-temperature anneal ($\sim$673 K) is effective in both the redistribution of cations to their equilibrium sites and the lowering of the defect concentration. Contamination of the resulting ferrite is found to be restricted to small amounts of Fe from the steel cylinder and balls that are readily incorporated into the ferrite structure during milling. We find the Fe contamination to scale linearly with milling duration; therefore exact stoichiometries can be obtained by tailoring the starting material ratio with Fe deficiencies.

It is interesting to note that the concept of alloying spinel ferrites through mechanical means was investigated as early as 1963.[4] Combining ZnO and Fe_2O_3 in an explosive compression, Kimura observed the formation of $ZnFe_2O_4$ via x-ray diffraction (XRD). Although much unreacted ZnO and Fe_2O_3 still remained, the success was a harbinger of things to come.

In 1978, Lefelshtel *et al.*[5] attempted to alloy ZnO and Fe_2O_3 in a ball mill, achieving partial conversion to $ZnFe_2O_4$ according to XRD, although peaks associated with the elemental oxides were still dominant. More recently, Kosmac and Courtney[6] subjected ZnO and Fe_2O_3 to HEBM and found that Zn ferrite became the dominant phase after 2.5 h. However, no trace of the spinel phase was seen by XRD after another 2.5 h milling. Similar results were achieved in the alloying of Ni ferrite from NiO and Fe_2O_3. Finally, in 1995, Jovalekic *et al.*[7] combined NiO and Fe_2O_3 and attributed all peaks in the XRD pattern to the spinel phase after milling 35 h, with little change in the XRD pattern upon subsequent milling. A surge of investigations in the last couple of years has resulted in similar use of elemental oxide powders to form $MnFe_2O_4$,[8] Fe_3O_4,[9] $MgFe_2O_4$,[10] and $Mn_{0.50}Zn_{0.50}Fe_2O_4$,[11–13] along with additional studies of mechanically alloyed $ZnFe_2O_4$.[14–18]

In addition to mixtures containing only elemental oxides, a carbonate ($ZnCO_3$) has been ball milled with Fe_2O_3 to form $ZnFe_2O_4$,[5] and $MnFe_2O_4$ and $Mn_{0.75}Zn_{0.25}Fe_2O_4$ have recently been produced by mechanically alloying elemental oxides with either a carbonate ($MnCO_3$) or an hydroxide ($Fe(OH)_3$).[17] In related experiments, precursor powder already in the spinel form was used to form $Co_{1-x}Fe_{2+x}O_4$ ($x=0$, 0.2, 0.5) via ball milling of Co_3O_4 with Fe_3O_4.[19,20]

The response of mechanosynthesized ferrites to heat treatment has also been investigated, both to determine their

[a]Author to whom correspondence should be addressed; electronic mail: harris@anvil.nrl.navy.mil

thermal stability and to gain insight into tailoring them for specific applications. Jovalekic *et al.*[7] compared the specific resistivity of $NiFe_2O_4$ generated from a sintered mixture of elemental oxides to that of identically sintered powders in which oxide mixtures had already been subjected to mechanical alloying, finding a dramatic decrease in resistivity with alloying duration. For example, powder subjected to 50 h mechanical alloying exhibits a postsintering resistivity 4 orders of magnitude less than that of the former method, showing promise for anticorrosion applications where small resistivities are desirable.

A reactivity study by Sepelak *et al.*[15] found that $ZnFe_2O_4$ produced via HEBM, as compared to $ZnFe_2O_4$ processed through a conventional high temperature anneal, exhibits greater high-temperature capability for both sulfur absorption and subsequent regeneration. Such improvements may benefit current environmentally conscious efforts to remove sulfur from coal gas.

Mechanical alloying has also been shown to yield a well-ordered spinel phase in ferrites at lower annealing temperatures and shorter duration than required in conventional ceramics methods.[8–10,13,15–17,20]

EXPERIMENT

Processing of MnZn ferrites, as described herein, was accomplished by combining MnO, ZnO, and Fe_2O_3, at a molar ratio of 1:1:2 in a steel cylinder of a SPEX 8000™ high-energy shaker mill. The cylinder was loaded with 5 g of starting materials (99.95 purity or better) in air with two 8 g and two 1 g steel balls and shaken at approximately 1200 Hz. To maintain a ball-charge mass ratio equal to 18:5 for all samples, the vial was cleaned and reloaded with 5 g of material for each milling trial. Milling operations were carried out for uninterrupted times ranging from 3 to 40 h. Long-range and short-range structural order of the milled samples were characterized using XRD and extended x-ray absorption fine structure (EXAFS), respectively. Samples milled for time greater than 20 h were found to consist predominantly of spinel ferrite and were subjected to additional characterization that included Mössbauer effect (ME), transmission electron microscopy, and superconducting quantum interference device (SQUID) magnetometry.

RESULTS AND DISCUSSION

XRD patterns collected from the milled mixtures are plotted in Fig. 1 with similar data from the starting mixture (i.e., $MnO+ZnO+Fe_2O_3$), and a MnZn ferrite standard.[21] A 2θ range that best illustrates the differences between the precursor oxide phases and the spinel ferrite is shown. These data have been multiplied by a scaling factor (denoted on the left hand side of the plots) and vertically offset to allow an improved visual comparison. With the exception of the α-Fe_2O_3 (104) and the ferrite (220) and (400) diffraction peaks, most of the intense diffraction features for the starting mixture and the ferrite overlap. Therefore, we will focus on the amplitude of these unique diffraction features to signal the presence and the degree of conversion from the binary oxides to the ferrite phase during milling. In Fig. 1, for milling times less than 6 h, the diffraction features corresponding to the binary oxide phases appear broadened and reduced in amplitude from the effects of the reduced particle size and the incorporation of strain and defects. These features retain their relative amplitudes and d spacing indicating that little ferrite conversion has occurred. However, for times greater than 6 h, one sees clear evidence of diffraction features that correspond with the ferrite (220) and (400) peaks. The increased amplitude and shift to higher d spacing of the most intense peak also suggests the presence of the ferrite (311) peak. As milling time is increased, the ferrite peaks grow in intensity and become further resolved at the expense of peaks corresponding to the precursor oxides. After times greater than 21 h, the only peaks detected above background are attributable to the ferrite phase. A lattice parameter of 8.421(6) Å is measured for the 21 h milled ferrite, which increases to 8.429(1) Å after 40 h of milling. An average particle size of 18.5 ± 1.0 nm was measured for the 40 h milled ferrites using the method of van Laue[22] in which instrumental broadening and particle shape are considered. Figure 2 plots the particle size evolution as a function of milling duration. The average particle size precipitously falls with milling duration from its maximum of ~60 nm (i.e., the starting mixture). A minimum of ~14 nm is reached after 10 h of milling. The particle size then starts to increase concurrent with the formation of nearly pure spinel ferrite. The

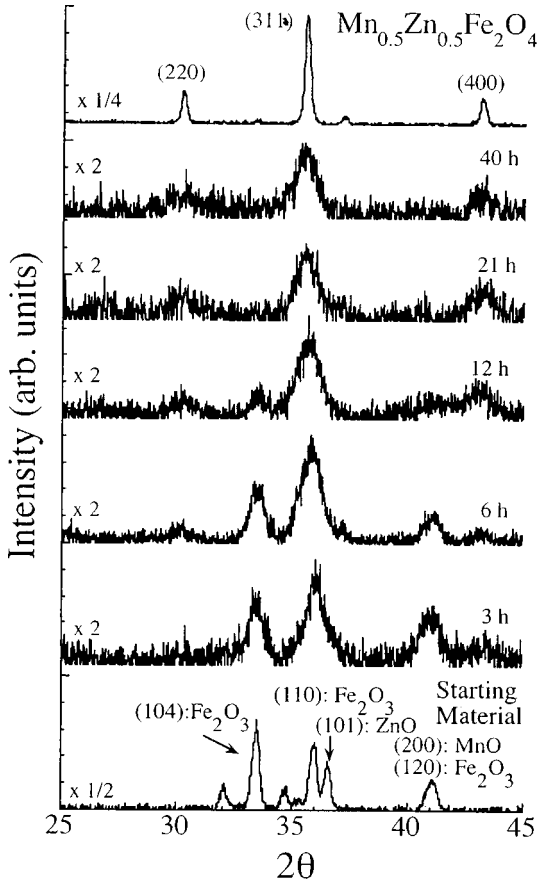

FIG. 1. Partial θ–2θ x-ray diffraction patterns of high-energy ball-milled oxide mixtures are shown with data from the starting mixture and the MnZn ferrite standard. (Cu $K\alpha$ radiation was employed in data collection).

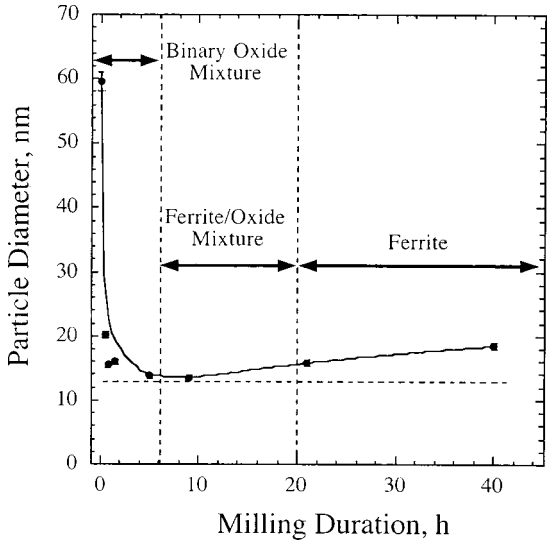

FIG. 2. Particle size as a function of milling duration. The solid line is presented as a guide to the eye, whereas the dashed line is presented as a zero slope reference. Particle size was determined via the method of von Laue (Ref. 22) in which instrumental broadening and particle shape are considered.

reason for this is unclear, although it may be due to a coarsening of the particles accompanying recrystallization. This may be assisted by the heating of the milling cylinder and charge.

Because XRD is more sensitive to medium- and long-range structural order, it is not the ideal technique to characterize nanoparticles. To address this deficiency, we have performed EXAFS measurement of the Fe, Mn, and Zn *K* absorption edges to complement these diffraction data. The EXAFS analysis is used to described the short-range structural environment around these cations.

EXAFS data were collected using the NRL X23B and the NIST X23A2 beamlines of the National Synchrotron Light Source at Brookhaven National Laboratory.[23] Analysis followed established procedures[24] leading to the Fourier transformation of EXAFS data to radial coordinate space (Å).

An analysis of the Fourier transformed data as a function of milling time shows that a 50% conversion from the precursor oxides to the spinel ferrite occurs after ~500 m (8.3 h) of continuous milling. Fourier transformed Fe, Mn, and Zn EXAFS data collected from the MnZn ferrite standard and the 40 h milled sample are shown in Figs. 3(a)–3(c), respectively. The data are plotted on two independent *y* axes to allow direct comparison between data sets without the loss of amplitude information. In this form, the positions of the Fourier peaks typically correspond to bond distances between the absorber and the backscatterers, while the amplitudes arise predominantly from the coordination and the atomic order of local atom is shells.[25] The Fourier peaks seen in Fig. 3 have been previously identified to correspond with atom pair correlations and/or multiple scattering paths within the ferrite unit cell.[26]

The structure of spinel ferrites consists of metallic cations occupying 8 of the 64 available tetrahedral (*A*) sites and 16 of the 32 available octahedral (*B*) sites within a close-

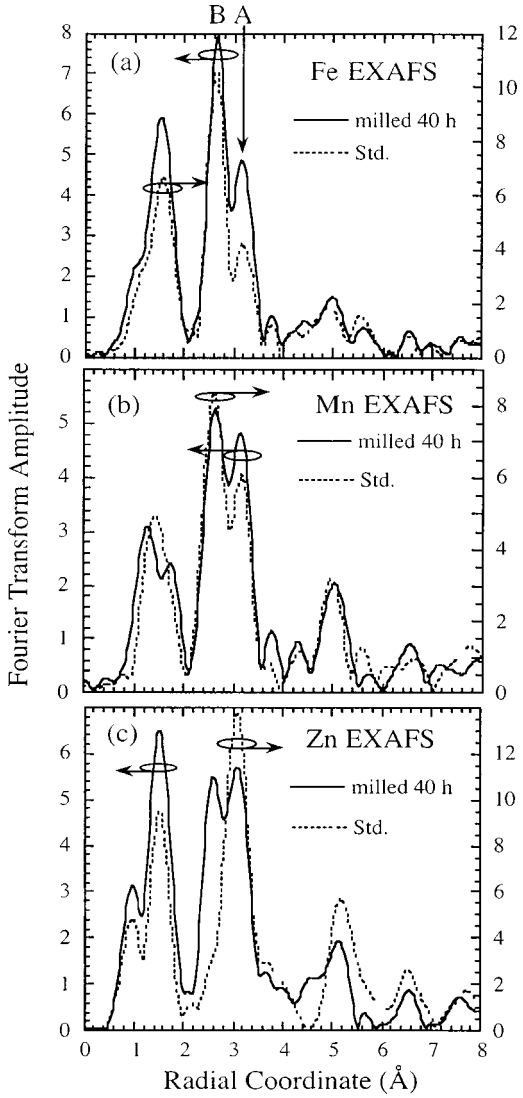

FIG. 3. Fourier transformed (a) Fe, (b) Mn, and (c) Zn EXAFS data from the ferrite produced after 40 h of milling and the MnZn ferrite standard. All data are k^3 weighted with k ranges of: (a) 2.85–13.4, (b) 3.1–11.7, and (c) 2.5–12.6 $Å^{-1}$.

packed oxygen lattice. These sites constitute individual sublattices leading to *A*–*A* and *B*–*B* antiferromagnetic interactions, and *A*–*B* interactions that are either antiferromagnetic or ferromagnetic depending upon the cation specie. The latter is typically dominant, leading to ferrimagnetism, although in some ferrites, such as conventionally processed $ZnFe_2O_4$, the absence of an *A*–*B* interaction results in antiferromagnetism at low temperatures. For any given ferrite, the valence and population of cations on the *A* and *B* sublattices principally determine the material's magnetic and electronic character. Recently, studies of both the cation distribution[11–13,17,18] and valence[13] in mechanically alloyed spinel ferrites have been performed.

The dominant feature in the Fourier transform that signifies unambiguous octahedral site (*B* site) occupancy of the absorber is the peak centered near 2.7 Å. This peak's amplitude arises solely from the scattering of 6 *B* cations and 6 anions centered near 2.97 Å.[27] The *A*-site occupancy is similarly indicated by a peak centered near 3.2 Å which arises

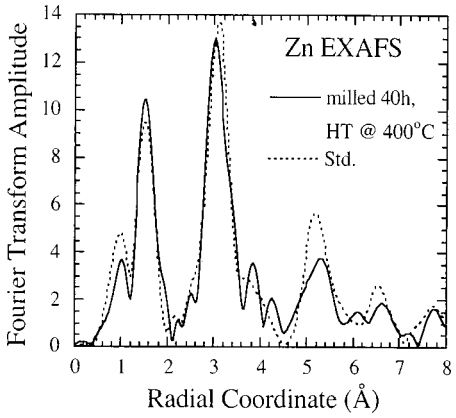

FIG. 4. Fourier transformed Zn EXAFS data from the milled sample after heat treatment at 673 K, and similar data from the standard. Notice that both data sets share a common *y* axis.

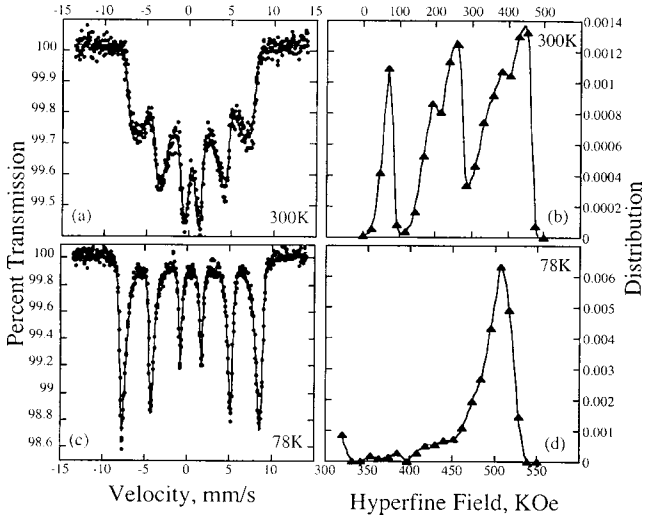

FIG. 5. Transmissions Mössbauer spectra acquired at: (a) 295 K and (c) 78 K for the sample milled for 40 h. Hyperfine field distributions resulting from the best fit of the data in panel (a) and (c) are presented in panels (b) and (d), respectively.

from the scattering of 12 octahedral-site (*B*-site) cations and 12 anions centered near 3.48 Å. [The differences between the bond distance and the radial coordinate of the Fourier transform (FT) peak in question is attributable to the electron phase shift that has not been incorporated into the data at this stage of analysis.] Modeling the data using multiple-scattering XAFS has showed the amplitudes of these peaks simulation codes[28] to reflect accurately the distribution of absorbing cations on the *A* and *B* sites.[29]

In comparing the *B:A* peak amplitude ratios of the sample milled 40 h to that of the standard, one sees that the milled sample possesses a higher fraction of Fe and Mn cations on the *A* sites, with an unusually high population of Zn cations on the *B* sites. Numerous studies have established that Fe and Mn cations may occupy both *A* and *B* sites depending upon the type and amount of other cations present as well as processing conditions. In contrast, it is rare to find a significant population of Zn cations on the *B* sites in equilibrium spinel structures. However, recent work by Hamdeh *et al.*[30] suggests that ball milling of partially inverted Zn ferrite aerogels increases *B*-site filling by Zn cations. The appearance of the *B* peak in Fig. 3(c) shows *unambiguously* that ball milling acts to distribute the Zn cations onto both sites. A heat treatment at 673 K is effective in facilitating a redistribution of cations to sites more closely resembling their equilibrium distribution. This is shown in Fig. 4, where the Fourier transformed Zn EXAFS data collected from the milled sample after heat treatment are plotted with similar data from the standard. In contrast to Fig. 3, these data share a common *y* axis and exhibit nearly the same peak amplitude and radial distributions. More importantly, the heat treatment has resulted in the removal of the signature *B*-site peak indicating that the Zn cations now only reside on the tetrahedral sites. The fact that the FT peak amplitudes are similar in the annealed sample and the standard indicates that the atomic disorder introduced to the ferrite during processing has been significantly, if not totally, removed. This indicates the ease in which one can ''repair'' the structure of the ferrite after milling.

Mössbauer spectra[31] collected at 295 and 78 K from the sample milled for 40 h are presented in Figs. 5(a) and 5(c). The spectrum collected at room temperature consists of broadened sextets that are clearly indicative of a distribution of hyperfine fields (HFFs). In these plots the data are presented as symbols and the solid curve represents the best fit to the data. The best fit was obtained using the method of Wivel and Morup[32] that represents the distribution of hyperfine fields with 22 sextets. In these fits the components of each sextet were held in the area ratio of 3:2:1:1:2:3 and the only variables were the isomer shift, the quadrupole shift, and the linewidth. The HFF distribution from the best fit of Fig. 5(a) [shown in Fig. 5(b)] can result either from a distribution of different cations in the local environment of each trivalent Fe cation, or from a distribution of small particle sizes with a range of magnetic HFFs (or both). Unfortunately, it is difficult to determine the relative importance of the two contributions to the HFF distribution. As might be expected, the distribution of HFFs sharpens at 78 K [Fig. 5(c)]. For the 40 h milled sample, the mean values of HFFs are 289 ± 5 and 487 ± 5 kOe at 295 and 78 K, respectively. The average isomer shift is 0.32 ± 0.01 mm/s at 295 K and 0.46 ± 0.01 mm/s at 78 K, values that are very typical of trivalent Fe in a spinel oxide lattice.[33] Further, as expected for a cubic like environment, the quadrupole shifts are very small, ranging from 0.07 ± 0.01 mm/s at 295 K to 0.00 ± 0.01 mm/s at 78 K. The fitting procedure assumes no texture in the absorber and no relaxation on the Mössbauer time scale. Because HEBM provides a broad particle size distribution, which often includes very small particles (i.e., <10 nm), it is surprising that we observe no clear evidence for a superparamagnetic component. However, we cannot rule out the presence of a superparamagnetic component from our analysis. Further, we detect no significant fraction of unreacted Fe–oxide phases (i.e., γ-Fe_2O_3, α-Fe_2O_3) that would have been clearly observable due to their unique HFFs.

Magnetization studies of the ferrite sample were performed using a Quantum Design™ SQUID magnetometer. Field dependent data were taken by sweeping the field while

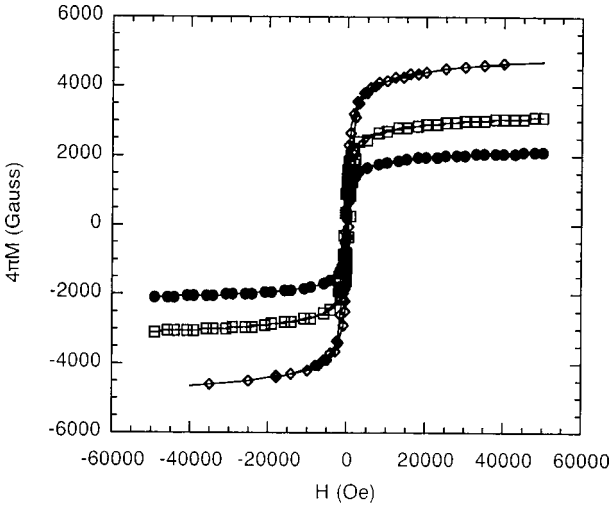

FIG. 6. Field dependent magnetization data for an as-milled sample of $Mn_{(0.5)}Zn_{(0.5)}Fe_2O_4$ at $T=300$ K (●) and at $T=6$ K (□). Also shown are data collected at 10 K for the milled sample after annealing (◇).

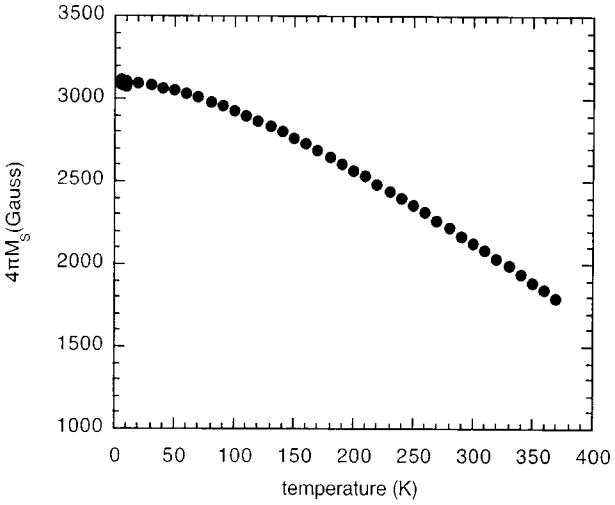

FIG. 8. Magnetization as a function of temperature.

holding the sample at fixed temperature, whereas the temperature dependence of the saturation magnetization was measured by cooling the sample in a large (5 T) applied field. Figure 6 plots the hysteresis curves taken at $T=300$ K and $T=6$ K for the as-milled sample together with data taken at $T=10$ K for the sample after subjecting it to a low temperature (523 K) anneal. The observed room temperature saturation magnetization for the as-milled sample is considerable less than the value of ~5000 G reported for polycrystalline samples of similar composition.[34] However, as shown in the figure, a low temperature anneal is effective in substantially increasing the saturation magnetization. This is consistent with the EXAFS results discussed earlier in which low-temperature anneals were shown effective in the redistribution of cations to their equilibrium lattice sites. Also evident in this figure is a small nonsaturating contribution to the magnetization at high fields. This is consistent with the presence of a superparamagnetic component. This is most likely attributable to the fact that the broad particle size distribution associated with HEBM process results in a finite fraction of small particles in the superparamagnetic regime. This result is consistent with the results of the ME measurements that showed a wide distribution of HFFs.

Figure 7 plots the low field behavior of the magnetization. While the room temperature data show no evidence for an irreversible magnetization, the low temperature behavior exhibits significant hysteresis with coercive fields of 600 and 450 Oe for the as-milled and annealed samples, respectively. This is consistent with the very broad ferromagnetic transition shown in Fig. 8 that plots saturation magnetization versus temperature. The Curie temperature reported for polycrystalline samples of this composition is approximately 400 K.[34] Our samples are measured to have a higher value similar to that reported by Tang *et al.* for fine particles of Mn ferrite.[35] We attribute this effect to the nonequilibrium distribution of cations possibly caused by surface oxidation.[36,37] The very broad ferromagnetic transition seen in Fig. 8 can be attributed to both the distribution of nonmagnetic Zn^{+2} cations on both sublattices as well as the broad distribution of small particle sizes exhibiting a range of magnetic hyperfine fields. The irreversibility seen at low temperatures is likely due to the magnetic ordering of these smaller particles at low temperatures.

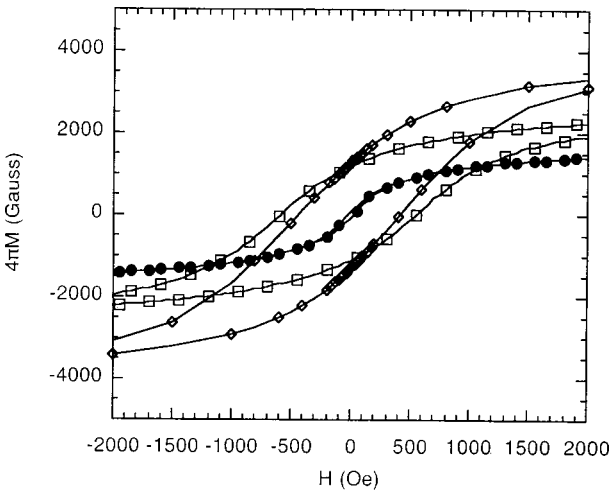

FIG. 7. Low field magnetization results for ball-milled $Mn_{(0.5)}Zn_{(0.5)}Fe_2O_4$ at $T=300$ K (●), and at $T=6$ K (□). Also shown are data collected at 10 K for the milled sample after annealing (◇).

SUMMARY

We have shown that nearly pure phase spinel ferrites can be fabricated via the high-energy ball milling of binary oxide precursors. This approach circumvents the deleterious high temperature anneals required by traditional processing routes. Although the final product suffers from a nonequilibrium cation distribution and a high concentration of defects, a low-temperature anneal is found to be effective in facilitating the redistribution of cations to their equilibrium sites and reducing the defect density. Challenges exist for the implementation of such a processing scheme at industrial scales.

ACKNOWLEDGMENTS

This work was supported by the Office of Naval Research. The authors thank Dr. J. C. Woicik for assistance in operating beamliner X23A2 at the NSLS. This work was performed in part at the National Synchrotron Light Source, which is sponsored by the U.S. Department of Energy. D.J.F., J.O.C., and E.E.C supported as a National Research Council Research Associate at the time of this research.

[1] C. R. Hendricks and V. W. R. Amarakoon, Ceram. Bull. **70**, 817 (1991).
[2] A. Goldman, *Modern Ferrite Technology* (Van Nostrand Reinhold, New York, 1990).
[3] C. C. Koch, Nanostruct. Mater. **9**, 13 (1997).
[4] Y. Kimura, J. Appl. Phys. **2**, 312 (1963).
[5] N. Lefelshtel *et al.*, Powder Technol. **20**, 211 (1978).
[6] T. Kosmac and T. H. Courtney, J. Mater. Res. **7**, 1519 (1992).
[7] C. Jovalekic *et al.*, Mater. Lett. **24**, 365 (1995).
[8] J. Ding *et al.*, J. Magn. Magn. Mater. **171**, 309 (1997).
[9] J. Ding *et al.*, J. Magn. Magn. Mater. **177–181**, 933 (1998).
[10] S. F. Moustafa and M. B. Morsi, Mater. Lett. **34**, 241 (1998).
[11] D. J. Fatemi *et al.*, J. Magn. Soc. Jpn. **22**, 80 (1998).
[12] D. J. Fatemi *et al.*, J. Appl. Phys. **83**, 6867 (1998).
[13] D. J. Fatemi *et al.*, J. Appl. Phys. **85**, 5172 (1999).
[14] V. Sepelak *et al.*, J. Solid State Chem. **101–103**, 1343 (1997).
[15] V. Sepelak *et al.*, Mater. Sci. Forum **235–238**, 139 (1997).
[16] V. Sepelak *et al.*, J. Solid State Chem. **135**, 52 (1998).
[17] D. Arcos *et al.*, Mater. Sci. Forum **269–272**, 87 (1998).
[18] P. Druska *et al.*, J. Solid State Chem. **146**, 13 (1999).
[19] J. Ding *et al.*, Appl. Phys. Lett. **65**, 3135 (1994).
[20] J. Ding *et al.*, Solid State Commun. **95**, 31 (1995).
[21] A MnZn-ferrite standard having the nominal stoichiometry $Mn_{0.5}Zn_{0.5}Fe_2O_4$ was processed by firing MnO, ZnO, and Fe_2O_3 for two successive 24 h anneals at 1250 °C. X-ray fluorescence measurements indicate that 8% of the Zn was lost during the firing process, with no detectable loss of Mn or Fe. XRD indicates a spinel with all diffraction peaks having relative intensities greater than 1% indexed to the powder diffraction pattern of Franklinite.
[22] M. von Laue, Z. Kristallogr. **64**, 115 (1926).
[23] The beamlines use double-crystal, fixed-exit monochromators, with Si(111) crystals in X23B and Si (311) crystals in X23A2. All spectra reported here were collected using the transmission technique. The storage ring current and energy at the time of data collection were 200–350 mA and 2.5 GeV, respectively. Samples consisted of powders spread uniformly onto adhesive tape with several layers constituting a single sample. The number of layers was chosen empirically to provide nearly one absorption length at the absorption edge being measured.
[24] D. E. Sayers and B. A. Bunker, in *X-ray Absorption: Principles, Applications, Techniques of EXAFS, SEXAFS, and XANES*, edited by D. C. Koningsberger and R. Prins (Wiley, New York, 1988), p. 211.
[25] The peak positions of the Fourier transformed data do not correlate directly with bond distances but are instead shifted to lower radial distances by an amount equal to the electron phase shift of the pair correlations contributing to the Fourier peak.
[26] V. G. Harris *et al.*, IEEE Trans. Magn. **31**, 3473 (1995).
[27] Bond distances were calculated assuming a lattice parameter of 8.39 Å and a.u.$=0.379\pm0.001$ Å.
[28] J. J. Rehr *et al.*, Phys. Rev. Lett. **69**, 3397 (1992).
[29] V. G. Harris *et al.*, Appl. Phys. Lett. **68**, 2082 (1996).
[30] H. H. Hamdeh *et al.*, J. Appl. Phys. **81**, 1851 (1997).
[31] The Mössbauer spectra were obtained on a constant-acceleration spectrometer which utilized a room temperature rhodium matrix Co^{57} source and was calibrated at room temperature with α-Fe foil. The Mössbauer absorbers contained 40 mg/cm^2 of the powdered material.
[32] C. Wivel and S. Morup, J. Phys. E **14**, 605 (1981).
[33] R. E. Vandenberghe and E. D. Grave, in *Mossbauer Spectroscopy Applied to Inorganic Chemistry*, edited by G. J. Long and F. Grandjean (Plenum, New York, 1989), Vol. 3, pp. 59–182.
[34] *Handbook of Microwave Ferrite Materials*, edited by Wilhelm H. von Aulock (Academic, New York, 1965), pp. 303–351.
[35] Z. X. Tang *et al.*, Phys. Rev. Lett. **67**, 3602 (1991).
[36] V. G. Harris *et al.*, J. Magn. Soc. Jpn. **22**, 157 (1998).
[37] P. J. van der Zaag *et al.*, Phys. Rev. B **51**, 12009 (1995).